Published for SISSA by Springer

Received: December 22, 2012
Accepted: February 13, 2013
Published: March 18, 2013

Thermal correlators in the ρ channel of two-flavor QCD

Bastian B. Brandt,[b,c] **Anthony Francis,**[b,d] **Harvey B. Meyer**[a,b,d] **and Hartmut Wittig**[a,b,d]

[a] *PRISMA Cluster of Excellence, Johannes Gutenberg-Universität Mainz, D-55099 Mainz, Germany*

[b] *Institut für Kernphysik, Johannes Gutenberg-Universität Mainz, D-55099 Mainz, Germany*

[c] *Institut für theoretische Physik, Universität Regensburg, D-93040 Regensburg, Germany*

[d] *Helmholtz Institut Mainz, Johannes Gutenberg-Universität Mainz, D-55099 Mainz, Germany*

E-mail: brandt@kph.uni-mainz.de, francis@kph.uni-mainz.de, meyerh@kph.uni-mainz.de, wittig@kph.uni-mainz.de

Abstract: We present a lattice QCD calculation with two dynamical flavors of the isovector vector correlator in the high-temperature phase. We analyze the correlator in terms of the associated spectral function, for which we review the theoretical expectations. In our main analysis, we perform a fit for the difference of the thermal and vacuum spectral functions, and we use an exact sum rule that constrains this difference. We also perform a direct fit for the thermal spectral function, and obtain good agreement between the two analyses for frequencies below the two-pion threshold. Under the assumption that the spectral function is smooth in that region, we give an estimate of the electrical conductivity.

Keywords: Quark-Gluon Plasma, Lattice QCD, Thermal Field Theory, Sum Rules

ArXiv ePrint: 1212.4200

doi:10.1007/JHEP03(2013)100

JHEP03(2013)100

Contents

JHEP03(2013)100

1 Introduction

The properties of strongly interacting matter under extreme conditions are the subject of intensive experimental and theoretical investigation. A comprehensive picture of a state of matter requires not only the knowledge of equilibrium properties such as the equation of state and static susceptibilities, but also an understanding of its transport properties.

In the high-temperature phase of QCD, the transport coefficients (the shear and bulk viscosities as well as the electrical conductivity) have been calculated perturbatively to full leading order in the strong coupling α_s [1–3]. However, in the range of temperatures that can be reached in heavy ion collisions, the perturbative uncertainty remains large. Phenomenologically, the observation of large elliptic flow in heavy ion collisions at RHIC and at the LHC hints at a small shear viscosity ([4, 5] and references therein). Furthermore, the measured spectrum of dileptons is related to the spectral functions of the electromagnetic current, integrated over the history of the expanding system [6].

Any reliable calculation of a transport coefficient of QCD at a temperature of a few hundred MeV would be extremely valuable. It therefore makes sense to undertake a calculation in the comparatively easiest possible channel. For a lattice QCD approach, the

spectral function of the isovector vector current is perhaps the most accessible channel. First, the correlation function is evaluated via a single, connected Wick contraction, allowing for a good signal-to-noise ratio in the Monte-Carlo simulation. Second, the light quarks do not introduce a new dynamical scale into the problem in the way that heavy quarks do, which typically requires the use of an effective field theory. Third, the corresponding vacuum spectral function, being extremely well known experimentally due to decades of measurements of the R ratio and of τ decays (see for instance [7]), provides a useful reference.

Here we present the first lattice calculation of the Euclidean isovector vector correlator in the high-temperature phase of QCD with dynamical quark flavors and analyze it in terms of the spectral function. We adopt an approach used previously in the bulk channel [8], which consists in analyzing directly the difference of the thermal and vacuum correlators. Moreover, we exploit a recently derived sum rule which constrains the integral over the difference of spectral functions (divided by frequency) to vanish. We compare our results at finite lattice spacing with a recent analysis performed in the continuum limit of quenched QCD [9].

In spite of the technically favorable properties of the channel, determining the vector spectral function with frequency resolution $\Delta\omega \ll T$ remains a numerically ill-posed problem (see for instance the discussion in [10]). Our main goal in this paper is therefore of qualitative nature and consists in determining the gross features of the thermal spectral function, in particular in which frequency bins (of width $\Delta\omega \gtrsim 2T$) it under- or overshoots the vacuum spectral function.

2 Theoretical expectations for the spectral function

In this section we set up our notation and define the relevant correlation functions. We summarize the theoretical expectations for these correlators and the associated transport properties.

2.1 Definitions

Our primary observables are the Euclidean vector current correlators,

$$G_{\mu\nu}(\tau,T) = \int d^3x \, \langle J_\mu(\tau,\boldsymbol{x}) \, J_\nu(0)^\dagger \rangle \,, \tag{2.1}$$

with $J_\mu(x) \equiv \frac{1}{\sqrt{2}} \big(\bar{u}(x)\gamma_\mu u(x) - \bar{d}(x)\gamma_\mu d(x)\big)$ the isospin current. The expectation values are taken with respect to the equilibrium density matrix $e^{-\beta H}/Z(\beta)$, where $\beta \equiv 1/T$ is the inverse temperature. The quark number susceptibility is defined as

$$\chi_s \equiv -\int d^4x \, \langle J_0(x) J_0(0) \rangle = -\beta \int d^3x \, \langle J_0(\tau,\boldsymbol{x}) J_0(0) \rangle. \tag{2.2}$$

Due to charge conservation, the two correlators of interest are exactly related via

$$G_{ii}(\tau,T) = \chi_s T + G_{\mu\mu}(\tau,T) \quad . \tag{2.3}$$

JHEP03(2013)100

The Euclidean correlators have the spectral representation

$$G_{\mu\nu}(\tau,T) = \int_0^\infty \frac{d\omega}{2\pi}\, \rho_{\mu\nu}(\omega,T)\, \frac{\cosh[\omega(\beta/2-\tau)]}{\sinh(\omega\beta/2)}\,. \tag{2.4}$$

For a given function $\rho(\omega,T)$, the reconstructed correlator is defined as

$$G^{\rm rec}(\tau,T;T') \equiv \int_0^\infty \frac{d\omega}{2\pi}\, \rho(\omega,T')\, \frac{\cosh[\omega(\frac{\beta}{2}-\tau)]}{\sinh(\omega\beta/2)}\,. \tag{2.5}$$

It can be interpreted as the Euclidean correlator that would be realized at temperature T if the spectral function was unchanged between temperature T and T'. For $T'=0$ it can be directly obtained from the zero-temperature Euclidean correlator via [8]

$$G^{\rm rec}(\tau,T) \equiv G^{\rm rec}(\tau,T;0) = \sum_{m\in\mathbb{Z}} G(|\tau+m\beta|, T=0). \tag{2.6}$$

2.2 Theoretical predictions

The isospin diffusion constant D is given by a Kubo formula in terms of the low-frequency behavior of the spectral function,

$$D\chi_s = \frac{1}{6}\lim_{\omega\to 0}\frac{\rho_{ii}(\omega,T)}{\omega}. \tag{2.7}$$

In the thermodynamic limit, the subtracted vector spectral function obeys a sum rule (see [11] section 3.2),

$$\int_{-\infty}^{\infty}\frac{d\omega}{\omega}\,\Delta\rho(\omega,T) = 0, \qquad\qquad \Delta\rho(\omega,T) \equiv \rho_{ii}(\omega,T) - \rho_{ii}(\omega,0). \tag{2.8}$$

This sum rule is based on two ingredients. Firstly, the two-point function of a spatial component of the vector current at vanishing four-momentum can be interpreted as the susceptibility of the isospin charge at zero temperature in a system with one short spatial periodic dimension of length β. As long as the correlation lengths are finite, this susceptibility vanishes. Secondly, subtracting the same quantity in the infinite-volume vacuum enables one to write a convergent sum rule in ω for the susceptibility. It is well known from the operator-product expansion that the difference of spectral functions in eq. (2.8) falls off as $1/\omega^2$ at large frequencies, see [12, 13] for explicit calculations.

For non-interacting massive quarks in the fundamental representation of the SU(N_c) color group, the vector spectral function is diagonal in flavor space and takes the form

$$\begin{aligned}\rho_{ii}(\omega,T) \,=\, & 2\pi\chi_s\langle v^2\rangle\omega\delta(\omega) \\ & + \frac{N_c}{2\pi}\theta(\omega-2m)\left[1-\left(\frac{2m}{\omega}\right)^2\right]^{\frac{1}{2}}\left[1+\tfrac{1}{2}\left(\frac{2m}{\omega}\right)^2\right]\omega^2\tanh\frac{\omega}{4T}.\end{aligned} \tag{2.9}$$

The next-to-leading order has been computed very recently [14]. At large frequencies the radiative corrections $(1+\alpha_s/\pi+\dots)$ to the coefficient of the ω^2 term are temperature independent and known to order α_s^4 [15] (for quark mass effects in the vacuum, see [16]). The

JHEP03(2013)100

	$m=0$	$m \gg T$
χ_s	$\frac{N_c}{3}T^2$	$\frac{4N_c}{T}\left[\frac{mT}{2\pi}\right]^{3/2} e^{-m/T}$
$\langle v^2\rangle$	1	$3T/m$.

Table 1. The static susceptibility and mean square velocity in the massless and in the heavy-quark limits.

susceptibility and the mean squared transport velocity $\langle v^2\rangle$ have the following expressions,

$$\chi_s = 4N_c\beta \int \frac{d^3\boldsymbol{p}}{(2\pi)^3}\, f_{\boldsymbol{p}}(1-f_{\boldsymbol{p}}) \tag{2.10}$$

$$\chi_s\langle v^2\rangle = 4N_c\beta \int \frac{d^3\boldsymbol{p}}{(2\pi)^3}\, f_{\boldsymbol{p}}(1-f_{\boldsymbol{p}})\, \frac{\boldsymbol{p}^2}{E_{\boldsymbol{p}}^2} \tag{2.11}$$

with $f_{\boldsymbol{p}} = 1/[e^{\beta E_{\boldsymbol{p}}}+1]$ the Fermi-Dirac distribution and $E_{\boldsymbol{p}} = \sqrt{\boldsymbol{p}^2+m^2}$. It is now straightforward to check that the sum rule (2.8) is verified in the free theory. The positive contribution of the transport peak (the $\omega\delta(\omega)$ contribution in the free theory) is compensated by a deficit of the thermal spectral function at intermediate frequencies, $\omega = \mathcal{O}(T)$ in the massless case. The susceptibility and mean square velocity have simple expressions in the massless and in the heavy-quark limits, see table 1.

Beyond the non-interacting theory, at weak coupling kinetic theory predicts the presence of a narrow transport peak in the spectral function at $\omega = 0$, whose width and height are related to the properties of the quasi-particles. Introducing a separation scale Λ between the transport time scale and the thermal time-scale, the area under the transport peak is, to leading order, preserved by the interactions [17],

$$\mathcal{A}(\Lambda) = \int_{-\Lambda}^{\Lambda} \frac{d\omega}{2\pi}\frac{\rho_{ii}(\omega,T)}{\omega} = \chi_s\langle v^2\rangle. \tag{2.12}$$

The width of the transport peak however becomes finite. In the heavy-quark limit for instance, the Langevin effective theory predicts a Lorentzian form [17]

$$\rho_{ii}(\omega,T) = \chi_s\langle v^2\rangle \frac{2\eta\,\omega}{\omega^2+\eta^2}, \qquad\qquad m \gg T, \tag{2.13}$$

where η is the 'drag coefficient', $1/\eta = D\frac{m}{T}$. The case of massless quarks can be treated with the Boltzmann equation [1, 18, 19], with a form of the spectral function qualitatively similar to eq. (2.13) and a drag coefficient given by

$$\eta = \frac{g^2}{8\pi} C_F m_D^2 \log(T/m_D), \tag{2.14}$$

with m_D the Debye mass and $C_F = \frac{N_c^2-1}{2N_c}$.

Finally, in contrast with the weak-coupling analysis outlined above, it is worth mentioning that at least one theory is known where the vector spectral function does not

JHEP03(2013)100

exhibit a transport peak. In the strongly coupled $\mathcal{N} = 4$ super-Yang-Mills theory, the spectral function of the R-charge correlator reads [20],

$$\rho^R_{ii}(\omega, T) = \frac{3\chi_s}{2\pi}\left(\frac{\omega}{T}\right)^2 \frac{\sinh\frac{\omega}{2T}}{\cosh\frac{\omega}{2T} - \cos\frac{\omega}{2T}}\,. \tag{2.15}$$

The static susceptibility is given by $\chi_s = \frac{N_c^2 T^2}{8}$, and the diffusion constant by $D = \frac{1}{2\pi T}$.

2.3 Connection with electromagnetic observables

The electrical conductivity σ is extracted from the correlator of the current $J^{\rm em}_\mu = \sum_f Q_f \bar{q}_f \gamma_\mu q_f$. If the quark species are degenerate, this correlator is given by the sum of a contribution proportional to $\sum_f Q_f^2$ and a contribution proportional to $(\sum_f Q_f)^2$. At high frequencies, the latter contribution to the spectral function is predicted to be small in perturbative QCD. Assuming that this contribution is also small at low frequencies, we have for the electrical conductivity in $N_{\rm f} = 2$ QCD

$$\sigma = C_{em} D \chi_s. \tag{2.16}$$

with $C_{em} = \sum_{f=u,d} Q_f^2 = 5/9$. If one further assumes that σ is fairly insensitive to the quark mass, and that the transport properties are not significantly affected by the presence of virtual strange quark pairs, the electrical conductivity in $N_f = 2+1$ QCD is given by eq. (2.16) with $C_{em} = \sum_{f=u,d,s} Q_f^2 = 2/3$.

The phenomenological significance of the electromagnetic spectral function is that the dilepton rate and the real-photon production rate are given by [18, 21]

$$\frac{{\rm d}N_{l^+l^-}}{{\rm d}\omega {\rm d}^3p} = C_{em}\frac{\alpha_{em}^2}{6\pi^3}\frac{\rho_{\mu\mu}(\omega, \boldsymbol{p}, T)}{(\omega^2 - \boldsymbol{p}^2)(\mathrm{e}^{\omega/T} - 1)}\quad , \tag{2.17}$$

$$\lim_{\omega\to 0}\omega\frac{{\rm d}R_\gamma}{{\rm d}^3p} = \frac{3}{2\pi^2}\sigma(T) T \alpha_{em} \tag{2.18}$$

where α_{em} is the electromagnetic fine structure constant.

2.4 Phenomenology of the ρ resonance

In the vacuum, the QCD spectral function of the electromagnetic current is well measured via the $R(s = \omega^2)$ ratio. The ρ meson completely dominates the spectral function up to about $\omega = 1$GeV. We work in the exact isospin symmetric theory and therefore ignore issues related to isospin breaking and $\rho - \omega$ mixing, see [22] for a recent reference.

Since we are working with the isospin current, we should restrict ourselves to final hadronic states with $I = 1$. The $R_1(s)$ ratio is defined analogously to $R(s)$ with this restriction. A rough parametrization of the experimentally measured $R_1(s)$ ratio was given in ref. [11], eq. (93). The spectral function in our normalization is related to the R_1 ratio via

$$\rho_{ii}(\omega, 0) = \frac{1}{\pi} R_1(\omega^2)\,\omega^2. \tag{2.19}$$

We can now make a simple argument about the thermal spectral function based on the exact sum rule (2.8), the kinetic theory sum rule (2.12) and the experimentally known

JHEP03(2013)100

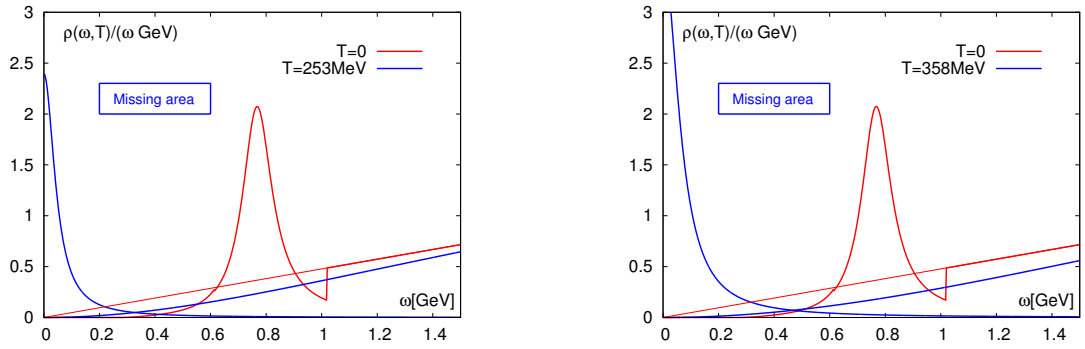

Figure 1. The phenomenological isovector vector spectral function ρ_{ii} in the vacuum compared to the leading-order weak-coupling prediction for the spectral function in the high-temperature phase. The Born term is as given in eq. (2.9) for $m = 0$ and we have represented the transport peak around $\omega = 0$ by a Lorentzian with a width matched to [18] for $\alpha_s = 0.3$ and an area determined by $\langle v^2 \rangle = 1$ together with $\chi_s/\chi_s^{\rm SB} = 0.88$ and 0.9 respectively for the left and right panel (table 2 and [23]). The thin red line represents the vacuum spectral function for non-interacting massless quarks. The weak-coupling thermal spectral functions must receive additional contributions of the size given by the 'missing area' rectangle in order to satisfy the sum rule (2.8).

vacuum spectral function. Using the parametrization of [11], the area under the vacuum spectral function up to $\omega = 1$GeV is about

$$\mathcal{A}_\rho \equiv \int_0^{1.0\text{GeV}} \frac{d\omega}{\pi} \frac{\rho_{ii}(\omega,0)}{\omega} \approx 0.114\text{GeV}^2. \tag{2.20}$$

By contrast, the corresponding area for free massless quarks at zero temperature is

$$\mathcal{A}_{\rm free} = 0.076\text{GeV}^2. \tag{2.21}$$

Taking into account the physical light quark masses changes this value by a negligeable amount.

In the free theory, the sum rule (2.8) is satisfied. Now switching on interactions between quarks, let us assume for the sake of the argument that in the high temperature phase they can be described perturbatively. In the small frequency region, interactions turn the delta function in eq. (2.9) into an approximate Lorentzian curve [18], *preserving its area to leading order*. This is the content of a kinetic theory sum rule [17]. In the vacuum, interactions have a dramatic effect on the spectral function, due to chiral symmetry breaking and confinement, and convert its area up to 1GeV from $\mathcal{A}_{\rm free}$ to $\mathcal{A}_\rho$. Since the sum rule (2.8) must still be satisfied, the weak-coupling spectral function in the high-temperature phase must acquire an additional area of

$$\mathcal{A}_{\rm missing} = \mathcal{A}_\rho - \mathcal{A}_{\rm free} \approx 0.038\text{GeV}^2. \tag{2.22}$$

Note that at very high temperatures, the area (2.22) is negligible compared to the area $\mathcal{A}(\Lambda) = \chi_s \langle v^2 \rangle$ under the transport peak, which grows as T^2. However, consider the situation at $T = 253$MeV (the temperature at which we have computed the correlator on

JHEP03(2013)100

the lattice, see the next section). Assuming the existence of a transport peak, its area $\mathcal{A}(\Lambda)$ is about 0.056GeV^2, if we correct for the fact that the static isospin susceptibility is about 12% below its Stefan-Boltzmann limit χ_s^{SB} (see table 2 and [23]). The area missing from the weak-coupling spectral function is thus comparable in size to the transport peak area at this temperature. The argument is illustrated in figure (1).

At $\omega \gg T$, the difference of spectral functions $\Delta\rho(\omega, T)$ can be analyzed with the operator product expansion (see [13, 24] and References therein). The lowest-dimensional gauge-invariant operators are of dimension four, and therefore the asymptotic behavior is $\Delta\rho(\omega, T) \propto 1/\omega^2$ (possibly up to logarithms). According to eq. (4.1) of ref. [24], the leading term of order $1/\omega^2$ is positive. However, at $T = 253\text{MeV}$ its contribution to the area under $\Delta\rho(\omega, T)/\omega$ is too small to explain the missing area (2.22).

In conclusion, at temperatures that are accessible in heavy-ion collisions, the sum rule (2.8) and the $R(s)$ ratio measurements place an important constraint on the thermal spectral function.

3 Lattice QCD data

All our numerical results were computed on dynamical gauge configurations with two light, mass-degenerate $\mathcal{O}(a)$-improved Wilson quark flavors. The configurations were generated using the MP-HMC algorithm [25, 26] in the implementation of Marinkovic and Schaefer [27] based on Lüscher's DD-HMC package [28]. The zero-temperature ensemble was made available to us through the CLS effort [29]. The gauge action is the standard Wilson plaquette action [30], while the fermions were implemented via the Wilson-Clover discretization with non-perturbatively determined clover coefficient c_{sw} [31].

We calculated correlation functions using the same discretization and masses as in the sea sector in two different ensembles. The first corresponds to virtually zero-temperature on a $64^3 \times 128$ lattice (labeled O7 in [32]) with a lattice spacing of $a = 0.0486(4)(5)\text{fm}$ [32] and a pion mass of $m_\pi = 270\text{MeV}$, so that $m_\pi L = 4.2$. Secondly we generated an ensemble on a lattice of size $64^3 \times 16$ with all bare parameters identical to the zero-temperature ensemble. In this way it is straightforward to compare the correlation functions respectively in the confined and deconfined phases of QCD. Choosing $N_\tau = 16$ yields a temperature of $T \simeq 250\text{MeV}$. Based on preliminary results on the pseudo-critical temperature T_c of the crossover from the hadronic to the high-temperature phase [33], the temperature can also be expressed as $T/T_c \approx 1.2$.

The renormalization of the vector correlator, calculated with the local vector current, assumes the form

$$G_{\mu\nu}(\tau, \beta, g_0) = Z_V^2(g_0)[1 + b_V(g_0) a m_q]^2 \left(G_{\mu\nu}^{lat}(\tau, \beta, g_0) + \dots \right). \tag{3.1}$$

The dots refer to $\text{O}(a)$ contributions from the improvement term proportional to the derivative of the antisymmetric tensor operator [34, 35] that we did not compute. We note however that perturbatively, the $\text{O}(a)$ contribution is suppressed by two powers of α_s. We use the non-perturbative value of Z_V provided by [36]. From the perturbative results of [35] we estimated the magnitude of the term $\sim b_V(g_0) a m_q$ to be of the order of 0.3%. Considering

JHEP03(2013)100

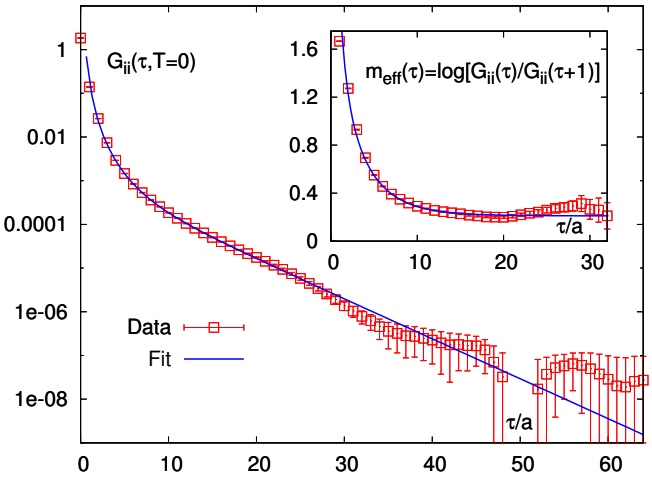

Figure 2. The vacuum vector correlator $G_{ii}(\tau, T = 0)$ computed on a lattice sized $64^3 \times 128$ and $m_\pi = 270$MeV, labeled O7 in [32]. The blue line denotes the fit result using eq. (3.2). The insertion shows the corresponding effective mass for $0 \leq \tau/a \leq 32$.

that the error of Z_V^2 is at the 1% level, we drop this contribution altogether in the following. Note that since we use the same bare parameters at zero and finite temperature, the multiplicative renormalization of the vector current only affects the corresponding correlation functions — and their difference — by an overall factor.

The vacuum correlator serves as a reference in this work. To fix the parameters of the lightest vector state in the finite volume of the simulation, we fitted the vacuum correlation function to an Ansatz of the form

$$G_{ii}(\tau, 0) = A_1 e^{-m_1 \tau} + \tfrac{3}{4\pi^2}\kappa_0 \, \exp(-\Omega\tau) \, \left(\Omega^2/\tau + 2\Omega/\tau^2 + 2/\tau^3\right), \tag{3.2}$$

which is the Laplace transform of

$$\frac{\rho_{ii}(\omega, 0)}{2\pi} = A_1 \, \delta(\omega - m_1) + \tfrac{3}{4\pi^2}\theta(\omega - \Omega) \, \kappa_0 \, \omega^2. \tag{3.3}$$

The finite-volume spectral function consists of Dirac δ functions. However, since many states contribute at short distances, the continuum in eq. (3.2) should be interpreted as resulting from the contributions of many energy eigenstates. In figure 2 we show the vacuum vector correlator $G_{ii}(\tau, T = 0)$ and the fit result. The insert shows the corresponding effective mass. The fit (performed in the interval $5 \leq \tau/a \leq 64$), clearly provides a good description of the data. For $\tau/a \gtrsim 32$ the quality of the data deteriorates and the signal is lost.

We will only use the result for the parameters A_1 and m_1 in the following. The question arises of the relation of these parameters to the infinite-volume spectral function. An answer is given by refs. [37, 38]. Assuming phenomenologically reasonable values of the ρ coupling to the $\pi\pi$ channel, the mass m_1 in fact appears to be within 10% of the (infinite-volume) ρ mass [37].

In addition we estimate the thermal isovector quark number susceptibility χ_s/T^2 from the last expression of eq. (2.2) at $\tau = \beta/2$ using again the local vector current. Note that

JHEP03(2013)100

	$64^3 \times 128$	$64^3 \times 16$	Ref.
$6/g_0^2$	5.50		
κ	0.13671		
$c_{\rm sw}$	1.7515		
Z_V	0.768(5)		[36]
a[fm]	0.0486(4)(5)		[32]
m_π[MeV]	270		[32]
T [MeV]		253(4)	
χ_s/T^2		0.871(1)	
A_1/T^3	4.42(31)		
m_1/T	3.33(5)		
κ_0	1.244(5)		
Ω/T	5.98(11)		

Table 2. The top part of the table shows the common quantities characterizing the zero-temperature and finite-temperature ensembles. In the lower part, the fit parameters for the vacuum correlator in units of $T = 253$MeV and the value of the (isospin) quark number susceptibility χ_s/T^2 are given. For more details on the generation of the $N_\tau = 128$ ensemble, see [32]. The number of configurations generated with $N_\tau = 16$ is 317.

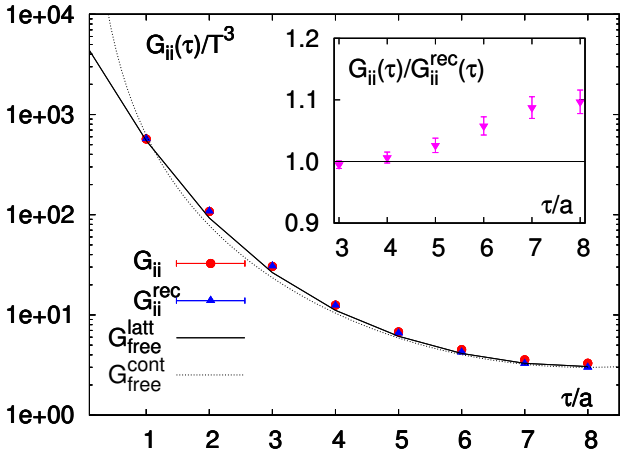

Figure 3. Thermal $G_{ii}(\tau)/T^3$ and reconstructed $G^{rec}_{ii}(\tau)/T^3$ vector correlators over Euclidean time separation τ compared to the free (continuum and lattice) cases. The reconstructed correlator was computed by applying eq. (2.5) to the data obtained from a lattice sized $N_\sigma = 64$ and $N_\tau = 128$. The insertion shows the ratio $G_{ii}(\tau)/G^{rec}_{ii}(\tau)$.

in the isovector channel, there are no disconnected diagrams. We checked the obtained value by fitting the correlator to a constant in the region $2 \leq \tau/a \leq 14$ and found only a negligible deviation. The parameters used in our lattice setup, the 'ρ-meson' parameters and the value of the static susceptibility are summarized in table 2.

JHEP03(2013)100

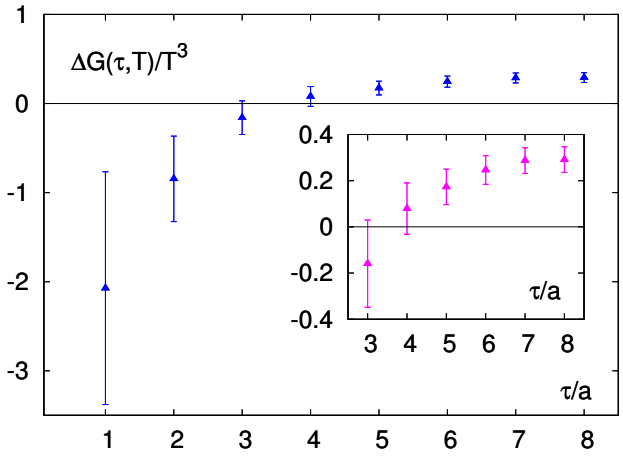

Figure 4. Difference $\Delta G(\tau,T)/T^3$ of the thermal vector correlator and the corresponding reconstructed correlator as a function of Euclidean time τ. The insertion shows $\Delta G(\tau,T)/T^3$ in the region $\tau/a \geq 3$.

τ	$G_{ii}(\tau)/T^3$	$G_{ii}^{rec}(\tau)/T^3$
4	12.534(94)	12.456(59)
5	6.775(65)	6.602(41)
6	4.510(51)	4.264(35)
7	3.569(45)	3.282(33)
8	3.300(44)	3.008(34)

Table 3. Results of the thermal and reconstructed correlation functions for $\tau/a \geq 4$. Note that all results have been renormalized using the value of Z_V in table 2 and normalized by T^3.

3.1 Thermal and vacuum correlators

In figure 3 we show the correlator $G_{ii}(\tau,T)$ computed at $T \simeq 250$MeV together with the corresponding free 'continuum' and free 'lattice discretized' correlation functions. In addition we show the reconstructed correlator $G_{ii}^{rec}(\tau)$ as obtained from eq. (2.6). The results for the thermal and reconstructed correlators for $\tau/a \geq 4$ can be found in table 3.

The reconstructed correlator lies somewhat lower than the thermal correlator. The insert in figure 3 displays the ratio $G_{ii}(\tau)/G_{ii}^{rec}(\tau)$ in order to make their relative τ dependence visible. For small Euclidean times $\tau < \beta/4$ this ratio is unity, above it increases monotonically until it levels off around the midpoint at about 10% above unity. A thermal modification of the spectral function has thus taken place (recall that the spectral function underlying $G_{ii}^{rec}(\tau)$ contains the bound states of the confined theory).

In figure 4 we show the difference

$$\Delta G(\tau,T) \equiv G_{ii}(\tau,T) - G_{ii}^{rec}(\tau,T) = \int_0^\infty \frac{d\omega}{2\pi} \Delta\rho(\omega,T) \frac{\cosh[\omega(\beta/2-\tau)]}{\sinh(\omega\beta/2)} \qquad (3.4)$$

of the thermal and the reconstructed correlators. Given that $\rho_{ii}(\omega,T)$ and $\rho_{ii}(\omega,T=0)$ have the same $\sim \omega^2$ behavior, this means we are subtracting non-perturbatively the

JHEP03(2013)100

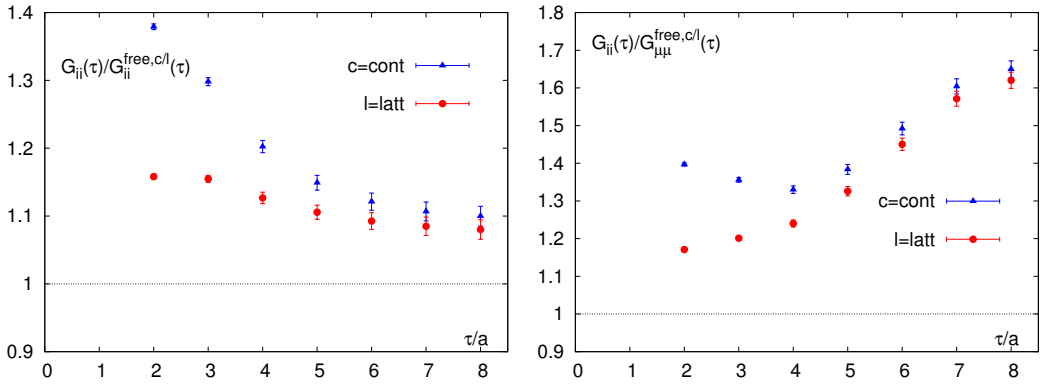

Figure 5. Left: The vector correlator $G_{ii}(\tau)$ at $T \simeq 250$MeV normalized by the free continuum and free discretized correlation functions $G_{ii}^{free,c/l}$. Right: The vector correlator $G_{ii}(\tau)$ normalized by the free (continuum/discretized) correlation functions $G_{\mu\mu}^{free,c/l}$.

ultraviolet tail of the spectral function. Using this difference we are therefore able to probe the change in the vector spectral function from the confined to the deconfined phase for frequencies $\omega \lesssim \mathrm{O}(T)$.

For small times, the difference (3.4) turns out to be negative, while it is positive for $\tau \geq \beta/4$. Note the errors decrease with increasing Euclidean time throughout the available range. We show a more detailed view of the region $\tau/a \geq 3$ in the insert of figure 4. Here the difference still exhibits a mild increase and levels off near the midpoint. The value it reaches at the midpoint is $\Delta G(\tau = \beta/2, T)/T^3 = 0.291(55)$.

3.2 Comparison with the free-quark correlator

In the previous subsection we compared the thermal correlator to its zero-temperature analogue. Now we analyze the thermal correlator in relation to the non-interacting case, which by asymptotic freedom corresponds to the regime of asymptotically high temperature. However, before discussing the departure of the simulation data from the non-interacting case, we address briefly the issue of cutoff effects.

Since we only have data at one lattice spacing, the value of the lattice correlator, viewed as an estimator of the continuum correlator, is necessarily ambiguous at some level due to cutoff effects. To estimate the size of this ambiguity, we show the ratio $G_{ii}/G_{ii}^{free,c/l}$ in figure 5(left), where c and l denote the analytically known free continuum and free lattice cases, respectively [39]. Concentrating on the ratio to the free *continuum* correlator we observe a decreasing trend throughout the entire available Euclidean time range, a behavior very similar to that seen in quenched studies [9]. Taking the ratio to the free *lattice* correlation function on the other hand the results are much flatter and almost constant at small times $\tau/a \leq 3$, while for $\tau/a \geq 5$ the two ratios track each other and are separated by a small shift of roughly 2%. The difference between the two curves comes from the fact that the free lattice correlation function takes into account the tree-level lattice artifacts.

To put this systematic uncertainty into perspective, we examine the ratio $G_{ii}/G_{\mu\mu}^{free,c/l}$ in the right panel of figure 5. The only difference between $G_{ii}^{free,c/l}$ and $G_{\mu\mu}^{free,c/l}$ is that the

JHEP03(2013)100

δ-function in the spectral function at $\omega = 0$ is absent in the latter. The difference between the left and right panel curves thus corresponds to the contribution of the transport peak. It is clear from the figure that this contribution is much larger than the cutoff effects present at tree-level for $\tau/a \geq 5$.

Returning now to the question of how much the thermal correlator differs from its non-interacting counterpart, we see that the simulation data lies 8 to 10% above the free lattice correlator. The sign of the effect corroborates our finding in section 2.4 that spectral weight is missing from the weak coupling spectral function.

3.3 Thermal moments of the correlator

Finally we compute also the ratio of thermal moments of the correlator [9]:

$$R^{(2,0)} = \frac{G^{(2)}}{G^{(0)}} = \frac{1}{2}\frac{\int d\omega\,(\omega/T)^2\rho(\omega)\overline{K}(\omega,T)}{\int d\omega\rho(\omega)\overline{K}(\omega,T)} \quad \text{where} \quad \overline{K}(\omega,T) = \frac{1}{2\pi\sinh(\omega/2T)} \quad . \tag{3.5}$$

This quantity can be extracted from the correlator data by combining the results of $(G_{ii}/G_{ii}^{free,c/l})(\tau = \beta/2) = G_{ii}^{(0)}/G_{ii}^{(0),free}$ and:

$$\Delta_{ii}(\tau) \equiv \frac{G_{ii}(\tau) - G_{ii}^{(0)}}{G_{ii}^{free}(\tau) - G_{ii}^{(0),free}} = \frac{G_{ii}^{(2)}}{G_{ii}^{(2),free}}\left[1 + \mathrm{O}((\beta/2-\tau)^2)\right]. \tag{3.6}$$

In the free case a straightforward computation [40] yields $R_{free}^{(2,0)} = 18.423$. Using this result together with our lattice data we obtain:

$$G_{ii}^{(0)}/G_{ii}^{(0),free} = 1.100(15)\,, \quad G_{ii}^{(2)}/G_{ii}^{(2),free} = 1.198(8) \quad \Rightarrow \frac{R^{(2,0)}}{R_{free}^{(2,0)}} = 1.089(30)\ , \tag{3.7}$$

where we neglected higher-order terms in the square bracket of eq. (3.6).[1] We see that the ratio $R^{(2,0)}$ of thermal moments is roughly 6–12% larger than the free result. As the ratio of second thermal moments is sensitive to changes in the low frequency region of the spectral function (see e.g. [9]), this observation could be due to a broadening of the δ-function form of the free theory.

4 Analysis of lattice correlators in terms of spectral functions

We begin with a simple but instructive analysis of the spectral function difference $\Delta\rho$. Section 4.2 contains the main analysis based on fits to the thermal part of the Euclidean correlator, and section 4.3 describes a fit directly to the thermal correlator. The results of the two fits are compared against each other and against previous quenched calculations in section 4.4.

4.1 A simple spectral analysis of the thermal part of the vector correlator

Based on the analysis of section 2.4, it is interesting to ask whether the Euclidean correlator can be described and the sum rule (2.8) satisfied solely by the transport peak and the ρ-meson contribution. For this purpose, we consider the following caricature of $\Delta\rho(\omega, T)$,

[1] Including the leading correction into a fit we find it to be poorly determined by the data, while the constant contribution remained unchanged within errors.

JHEP03(2013)100

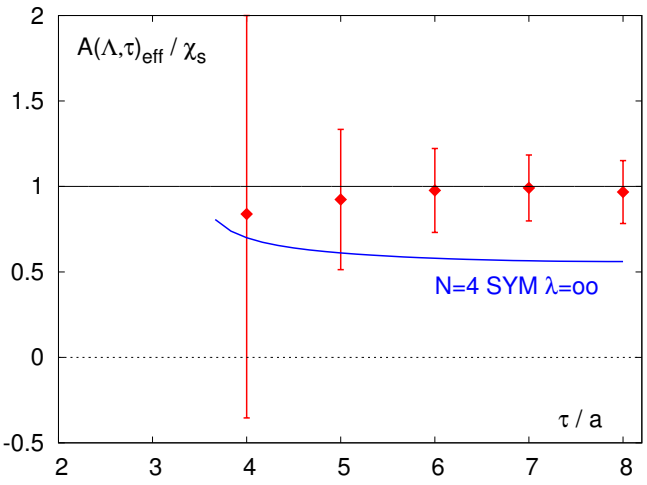

Figure 6. The effective area $\mathcal{A}(\Lambda,\tau)_{\rm eff}$, defined in eq. (4.3), normalized by the static susceptibility. The corresponding quantity in the strongly coupled SYM theory calculated from eq. (2.15) is also displayed for comparison.

where the sum rule has already been enforced,

$$\frac{\Delta\rho(\omega,T)}{2\pi} = C\,\omega\left(\delta(\omega) - \tfrac{1}{2}\delta(\omega - m_1)\right), \tag{4.1}$$

corresponding to the Euclidean correlator

$$\Delta G(\tau,T) = C\left(\frac{1}{\beta} - \frac{m_1}{2}\frac{\cosh m_1(\beta/2-\tau)}{\sinh m_1\beta/2}\right). \tag{4.2}$$

The mass m_1 is set equal to the value obtained by fitting the Ansatz (3.2) to the vacuum correlator and given in table 2. The kinetic theory sum rule (2.12) implies that C is an estimator for $\mathcal{A}(\Lambda)$, and from eq. (4.2) an effective value $\mathcal{A}(\Lambda,\tau)_{\rm eff}$ can thus be defined for every value of τ,

$$\mathcal{A}(\Lambda,\tau)_{\rm eff} = \frac{\Delta G(\tau,T)}{\left(\frac{1}{\beta} - \frac{m_1}{2}\frac{\cosh m_1(\beta/2-\tau)}{\sinh m_1\beta/2}\right)}. \tag{4.3}$$

The result is shown in figure 6. The quantity $\mathcal{A}(\Lambda,\tau)_{\rm eff}$ is well compatible with a constant value, implying that the Ansatz (4.1) already provides a good description of the lattice correlator. Moreover, the weak-coupling expectation that $\mathcal{A}(\Lambda,\tau)_{\rm eff}$ should be given by χ_s (up to quark mass effects reducing their average thermal velocity $\langle v^2\rangle$) is also well reproduced. The insensitivity of the Euclidean correlator to the width of the transport peak was first emphasized in [41, 42].

It should be noted that in this simple picture the prefactor of $\delta(\omega - m_1)$ in eq. (4.1) is about $-\chi_s m_1/2 = -1.45(2)T^3$, to be compared with the area $A_1 = +4.42(31)T^3$ obtained from the vacuum correlator (table 2). This observation means that the area under the thermal spectral function in the region $T \lesssim \omega \lesssim 4T$ cannot be negligible compared to A_1, confirming the conclusions drawn from phenomenology in section (2.4).

JHEP03(2013)100

It is interesting to confront the lattice data with the spectral function in the strongly coupled SYM theory, eq. (2.15). We therefore also plot the corresponding SYM function in figure (6). It lies lower than the lattice data, in spite of the fact that $\rho^{\rm R}_{ii}(\omega,T)/(\chi_s\omega^2)$ has the same large-frequency limit as $\rho^{\rm free}_{ii}(\omega,T)/(\chi_s^{\rm free}\omega^2)$ in QCD and also satisfies the sum rule (2.8). This comparison shows that the lattice data is not simultaneously compatible with the combination of (a) the functional form of the SYM spectral function and (b) the corresponding very low diffusion constant. The data is however perfectly compatible with the substitution of the delta function in eq. (4.1) by a flat (or even $\propto (1+\frac{1}{24}\omega^2/T^2)$ as in the SYM case) behavior of $\Delta\rho(\omega,T)/\omega$ up to about $\omega\approx 4T$, provided its area is adjusted appropriately.

In order to parametrize $\Delta\rho(\omega,T)$ systematically, including the expected contributions at high frequencies, we resort to the more sophisticated fits described in the next subsection. To anticipate the results, similar qualitative conclusions on the distribution of the spectral weight in $\Delta\rho(\omega,T)$ will be obtained.

4.2 Fit to the thermal part of the vector correlator

We proceed to investigate the behavior of the thermal part of the spectral function $\Delta\rho$ by fitting the difference of the thermal and the reconstructed correlator, see eq. (3.4). We know from the operator-product expansion that the difference of spectral functions falls off rapidly (as ω^{-2}) for $\omega\gg T$, and therefore focus on the region $\omega\lesssim {\rm O}(T)$ in order to choose a fit Ansatz. As described in the previous subsection, the fact that the data (displayed in figure 4) is positive at long distances and negative at short distances suggests that the thermal spectral weight exceeds the vacuum spectral weight at low frequencies and falls short of it at higher frequencies.[2]

We thus parametrize $\Delta\rho$ using the following Ansatz for $\omega\geq 0$:

$$\Delta\rho(\omega,T) = \rho_T(\omega,T) - \rho_B(\omega,T) + \Delta\rho_F(\omega,T), \tag{4.4}$$

$$\rho_B(\omega,T) = \frac{2c_B\, g_B\, \tanh(\omega/T)^3}{4(\omega-m_B)^2+g_B^2}, \tag{4.5}$$

$$\rho_{T,1}(\omega,T) = \frac{4c\,\omega}{(\omega/g)^2+1}, \qquad \rho_{T,2}(\omega,T) = \frac{4cT\tanh(\omega/T)}{(\omega/g)^2+1}, \tag{4.6}$$

$$\Delta\rho_F(\omega,T) = \rho_F(\omega,T) - \rho_F(\omega,0), \qquad \rho_F(\omega,T) = \frac{3}{2\pi}\kappa\,\omega^2\tanh\left(\frac{\omega}{4T}\right). \tag{4.7}$$

The bound state (B) and the transport peak (T) are represented by Breit-Wigner forms. Even such a simple Ansatz requires three parameters (c_B, g_B, m_B) to determine the bound state peak, two parameters (c, g) for the transport peak and one (κ) for the 'perturbative' contribution (F). We will therefore fix some of them using the vacuum correlator. In the following we set m_B equal to m_1, given in table 2, which we obtained from the exponential fit to the vacuum correlator. Note that the area under the bound state peak $\int dw\ \rho_B/\omega$ does not depend on the width g_B in the limit where it is small. The sensitivity of the Euclidean correlator to the latter parameter is very small. We therefore perform fits for

[2] A continuum extrapolation is really needed to confirm the behavior at short distances.

JHEP03(2013)100

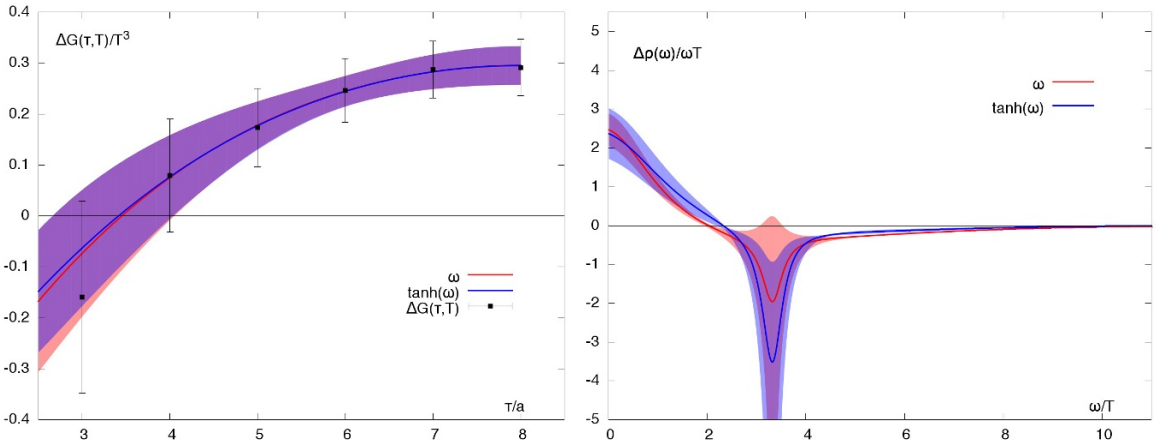

Figure 7. Left: Fits to $\Delta G(\tau,T)/T^3 \equiv [G_{ii}(\tau) - G_{ii}^{rec}(\tau)]/T^3$. The blue and red results differ by the form of transport peak in the Ansatz. The error bands are computed from the covariance matrix of the fit. Right: The resulting spectral functions for both Ansätze.

three fixed values of this parameter, and check the sensitivity of the result. We choose the values $g_B/T = 0.1, 0.5$ and 1.0, corresponding to $g_B \simeq 25, 125$ and 250MeV.

The tail $\sim T/\omega$ of the Ansatz $\rho_{T,1}$ violates the OPE prediction that $\Delta\rho \sim (T/\omega)^2$ at large frequencies. It has been argued in [43] that this might lead to an overestimate of the transport contribution. To avoid this problem we introduce the Ansatz 2, where $\omega \to T\tanh(\omega/T)$. This Ansatz possesses the correct asymptotic behavior, as well as the expected linear behavior in ω at small frequencies.

Finally, to complete the parametrization of $\Delta\rho(\omega)$, we include a weak-coupling term inspired by eq. (2.9) describing the subtraction of the large frequency parts of the thermal and vacuum spectral functions. This contribution $\rho_F(\omega,\kappa) \to 0$ vanishes exponentially as the frequency increases.

In the next step we fit the combined Ansätze of $\Delta\rho(\omega, c_B, g_B, m_B, c, g, \kappa)$ to the data, while at the same time satisfying the sum rule of eq. (2.8) to an accuracy of 10^{-8}. We limit ourselves to fitting the region $5 \le \tau/a \le 8$ only, in order to minimize the influence of cut-off effects, as discussed in section 3.1. With m_B determined by the vacuum correlator, we set g_B successively to the three different values mentioned above and fixed κ around unity, and fitted the parameters c, g and c_B. The errors and error bands shown in the following have been computed using the covariance matrix of the corresponding fit for fixed values of g_B and κ.

The resulting correlators and spectral functions are displayed in figure 7 for $g_B/T = 0.50$ and $\kappa = 1.10$ while the fitted parameters are given in table 4. In the left panel of figure 7 the data $\Delta G(\tau,T)$ is compared to the fits using $\rho_{T,1}(\omega)$ and $\rho_{T,2}(\omega)$ as transport contribution. We achieve a quasi-perfect description of the data for $\tau/a \ge 4$. The right panel shows that both Ansätze exhibit a substantial spectral weight around the origin and a negative contribution from the region of the ρ mass.

Focussing on Ansatz 2, the left panel of figure 8 shows the sensitivity of the fit result

JHEP03(2013)100

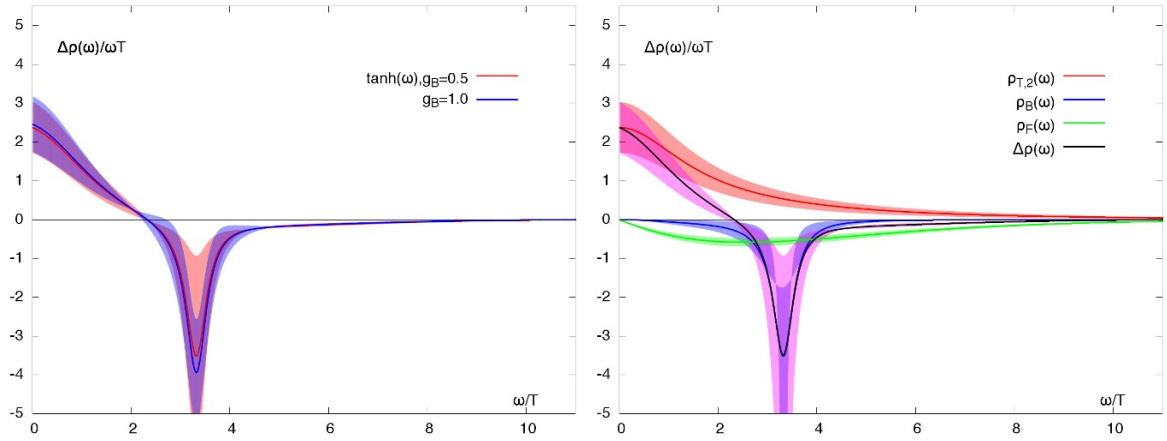

Figure 8. Left panel: the impact of changing the width of the peak representing the ρ resonance, $g_B = 0.5T$ and $g_B = 1.0T$. Right panel: the separate contributions $\rho_T(\omega)$, $\rho_B(\omega)$, $\rho_F(\omega)$ and the full result of the fitted spectral functions for the transport Ansatz $\rho_{T,2}$.

to varying the parameter g_B. Varying the width only has a small effect on the overall result. We also found little sensitivity to $\pm 15\%$ variations in κ. In order to understand what drives the parameters to their final fitted values, we also plot separately the three contributions appearing in eq. (4.4)–(4.7), including their respective error bands, in the right panel of figure 8. The contribution $\rho_F(\omega)$ mainly affects the intermediate frequency region around $\omega/T \simeq 2$. Its tail between $4 \leq \omega/T \leq 10$ is largely compensated by the tail of the Lorentzian centered at the origin, and this might well be what drives the width of the Lorentzian.

4.3 Weak-coupling inspired fit to the thermal vector

In contrast to the previous section, here we study directly the thermal vector correlator and its ratio of thermal moments $R^{(2,0)}$. We perform a fit inspired by the weak coupling form of the thermal spectral function,

$$\rho(\omega, T) = \rho_T(\omega, T) + \rho_F(\omega, T)\,, \tag{4.8}$$

where the form of the two contributions is defined in eq. (4.6) and (4.7). At a given temperature this Ansatz is characterized by three parameters (c, g, κ). We fit the full Ansatz $\rho(\omega, c, g, \kappa)$ to the thermal correlator $G_{ii}(\tau)$, while at the same time demanding that $R^{(2,0)}$ be reproduced. In this analysis the three parameters c, g and κ are fitted, and the fit range is $5 \leq \tau/a \leq 8$ as before.

The resulting correlators and spectral functions are shown in figure 9 with their fit parameters listed in table 4. The ratio $G_{ii}(\tau)/G^{\text{free}}_{\mu\mu}(\tau)$ in the left panel of figure 9 is well described by both versions $\rho_{T,1}$ and $\rho_{T,2}$ of the transport contribution for $\tau/a \geq 5$, while also the ratio of thermal moments (given on the far right of the plot) is reproduced. For $\tau/a < 5$ our Ansatz fails to reproduce these points within the error band, which we suspect is partly due to cutoff effects. The central value of the fit hardly changes if one extends the

JHEP03(2013)100

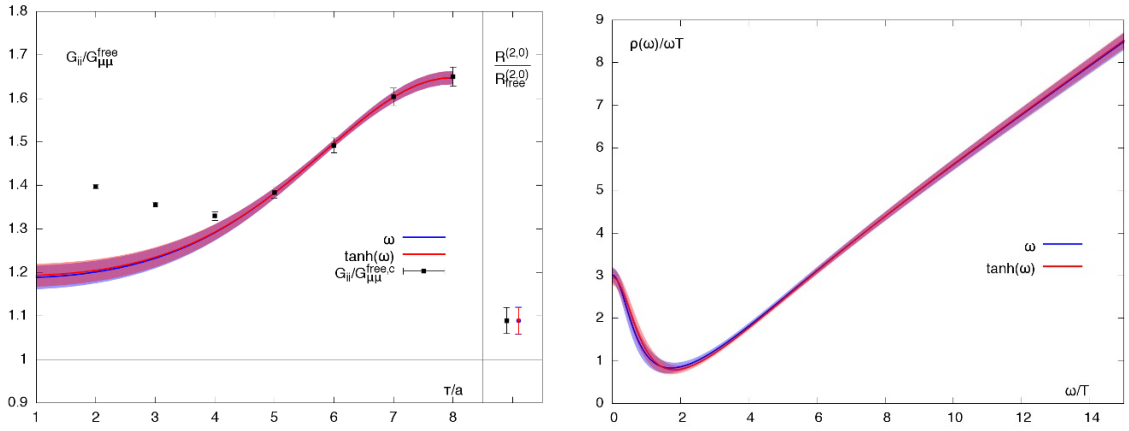

Figure 9. Left panel: fit results for $G_{ii}(\tau)/G^{free}_{\mu\mu}(\tau)$ using both Ansätze for the transport peak. The resulting ratio of thermal moments $R^{(2,0)}/R^{(2,0)_{free}}$ are displayed on the right side of the plot. Right panel: The corresponding spectral functions normalized by ωT.

$\Delta\rho(\omega, c, g, \kappa)$	c/T	g/T	c_B/T^3	$\mathcal{A}(\Lambda = 1.5T)/T^2$	$\langle v^2\rangle_{\text{eff}}$
$\rho_{T,1}(\omega, c, g)$	0.61(10)	1.22(26)	1.42(188)	0.702(201)	0.806(231)
$\rho_{T,2}(\omega, c, g)$	0.59(16)	5.7(10)	2.92(228)	0.764(244)	0.877(280)
$\rho(\omega, c, g, \kappa)$	c/T	g/T	κ	$\mathcal{A}(\Lambda = 1.5T)/T^2$	$\langle v^2\rangle_{\text{eff}}$
$\rho_{T,1}(\omega, c, g)$	0.75(4)	0.71(9)	1.186(27)	0.818(50)	0.939(57)
$\rho_{T,2}(\omega, c, g)$	0.74(5)	0.98(13)	1.192(26)	0.858(56)	0.985(64)

Table 4. Parameters obtained from both studies. Top: fitting $\Delta\rho(\omega, c, g, \kappa)$ to $\Delta G(\tau, T)$ with $g_B = 0.5T$ and $\kappa = 1.10$. Bottom: fitting $G_{ii}(\tau)$ to $\rho(\omega, c, g, \kappa)$. In both cases fits were done for two different Breit-Wigner peaks in the low frequency region, $\rho_{T,1}(\omega) \sim \omega$ and $\rho_{T,2}(\omega) \sim T\tanh(\omega/T)$. Additionally the resulting area of the transport region $\mathcal{A}(\Lambda)$ and the mean squared velocity $\langle v^2\rangle$ is given. For details see the text.

fit range to $\tau/a \geq 4.\text{XXX}$ In the future it would be interesting to repeat the calculation at several smaller lattice spacings while keeping the temperature fixed, as in [9].

On the right hand side of figure 9 we show the resulting spectral functions divided by ωT. Clearly both Ansätze give very similar results that lie within errors of each other. The thermal correlator is even less sensitive to the asymptotic behavior of the transport contribution in the Ansatz than in the difference of correlators studied in section 4.2.

4.4 Discussion

We now compare the results of the fits to $\Delta G(\tau, T)$ and $G_{ii}(\tau, T)$. Since the vacuum spectral function vanishes below $2m_\pi \approx 540\text{MeV}$ (in infinite volume), $\rho_{ii}(\omega, T)$ and $\Delta\rho(\omega, T)$ should be equal for $\omega < 2m_\pi \approx 2.1T$. We thus plot the spectral functions obtained from the two fits in this frequency region, see figure 10. Here we restrict ourselves to showing these results based on $\rho_{T,2}(\omega, T)$, as their theoretical foundation is more sound than those with $\rho_{T,1}(\omega, T)$. All curves are multiplied by a factor 1/6, which means that the intercept at $\omega = 0$ yields an estimate of $\sigma/C_{em}T$ with σ the electrical conductivity of the quark gluon plasma.

JHEP03(2013)100

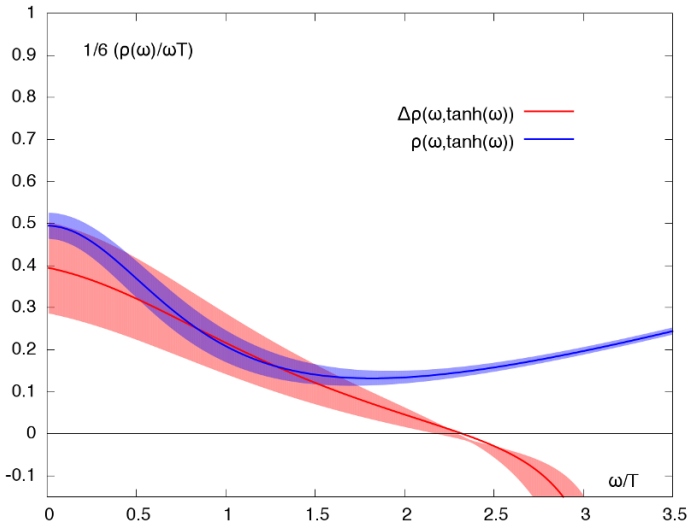

Figure 10. Comparison of the spectral functions obtained from analyzing (a) $\Delta G(\tau, T)$ and (b) $G_{ii}(\tau, T)$ using in both cases $\rho_{T,2}(\omega) \sim \tanh(\omega/T)$ in the low frequency region. All curves have been multiplied by a factor 1/6 and divided by ωT, entailing that the intercept at $\omega = 0$ yields an estimate of $\sigma/C_{em}T$.

The results obtained by fitting $G_{ii}(\tau, T)$ agree very well with the central values obtained by fitting $\Delta G(\tau, T)$, as summarized in table 4. The fit to $\Delta G(\tau, T)$ using the transport Ansatz $\rho_{T,2}(\omega)$ yields a slightly lower intercept. If we assume the spectral function to be as smooth around the origin as figure 10 suggests, we obtain the following estimate for the electrical conductivity of the quark gluon plasma at $T \simeq 250$MeV,

$$\frac{\sigma}{C_{em}T} = 0.40(12), \tag{4.9}$$

where $C_{em} = \sum_{f=u,d} Q_f^2 = 5/9$ for $N_f = 2$ and $C_{em} = \sum_{f=u,d,s} Q_f^2 = 2/3$ for $N_f = 2 + 1$, see section 2.3. It should be remembered that the Euclidean correlator can be perfectly well described by an infinitely narrow transport peak (corresponding to an infinite electrical conductivity), see section 4.1. Although obtained under a strong assumption, it is interesting to compare (4.9) to other lattice results obtained under similar assumptions. The following comparison is made with quenched results, since to our knowledge there are no previous dynamical QCD studies.

A quenched calculation using staggered fermions based on fitting the Fourier transform of the correlator obtained $\sigma/T = 7C_{em}$ [44] at $1.5 \leq T/T_c \leq 3.0$, where the pure SU(3) gauge theory critical temperature is around 290 MeV. A further study using staggered fermions and an analysis based on the maximum entropy method obtained $\sigma/T = 0.4(1)C_{em}$ [45]. Finally, a recent quenched study using Wilson-Clover fermions in the continuum limit obtained $0.33C_{em} \leq \sigma/T \leq 1C_{em}$ at $T \simeq 1.45T_c$ [9]. Our results using dynamical Wilson-Clover fermions at $N_\tau = 16$ are thus completely compatible with the recent quenched results.

JHEP03(2013)100

Even though the transport contribution extracted from our fits is not narrow and an interpretation in terms of kinetic theory (eq. (2.12)) is no longer rigorously motivated, we also compute the effective mean squared velocity of the quarks $\langle v^2 \rangle$. Choosing the scale parameter $\Lambda/T = 1.5$ and numerically integrating the fitted spectral functions we obtain $\mathcal{A}(\Lambda = 1.5T)$. Assuming eq. (2.12) and using the quark number susceptibility as given in table 2, it is straightforward to estimate an effective mean squared velocity $\langle v^2 \rangle_{\text{eff}}$. The results for $\mathcal{A}(\Lambda = 1.5T)$ and $\langle v^2 \rangle_{\text{eff}}$ are listed in table 4. For all fits we obtain reasonable values for $\langle v^2 \rangle_{\text{eff}}$ in the range $0.80 \lesssim \langle v^2 \rangle_{\text{eff}} \lesssim 0.99$. Thus, although we are not able to demonstrate or exclude the validity of the kinetic theory description, the values of the effective quark velocity extracted in this way are in line with its expectations. By contrast, the AdS/CFT spectral function (2.15) (which clearly cannot be described by kinetic theory) yields an effective quark velocity of $\langle v^2 \rangle_{\text{eff}} = 0.47$ for $\Lambda = 1.5T$.

Using the result for $\rho_{ii}(\omega, T)$ from the fit to $G_{ii}(\tau, T)$, it is straightforward to compute the production rate of thermal lepton pairs in the quark gluon plasma with two light dynamical quark flavors from eq. (2.17). The resulting rates are shown in figure 11. We give the low frequency behavior of $dN_{l^+l^-}/d\omega d^3p$ obtained from $\rho_{ii}(\omega, T)$ using the Ansatz 2 in the transport region. Comparing our results with the free (Born) rate (dashed line) and the hard thermal loop result (black line) with a thermal mass of $m_T/T = 1$ [46], we observe that for frequencies $\omega/T \lesssim 1.5$ our result is below the result from HTL, above this value however it follows it very closely.

The results shown in figure 11 correspond to a system at thermal equilibrium with $T \simeq 250\text{MeV}$. To make contact with results obtained in heavy ion collisions one has to take into account the real-time evolution of the volume of the system, using a hydrodynamic model along the lines of [47] (for a recent study of out-of-equilibrium photon and dilepton production using the AdS/CFT correspondence see [48, 49]).

5 Conclusion

In this paper we have obtained the isovector vector correlator in the high-temperature phase of two-flavor QCD at $T \simeq 250\text{MeV}$ as well as in the vacuum at the same set of bare parameters. This allowed us to analyze both the difference of the thermal and the vacuum correlator and the thermal correlator directly. In the former case the analysis is further constrained by an exact sum rule. Given the uncertainties inherent in trying to extract information on the spectral function from Euclidean correlators, the two methods give a consistent picture of the thermal spectral function in the low to moderate frequency range $\omega \lesssim 1.5T$.

The vacuum spectral function is known to receive a very large contribution from the ρ meson from experimental e^+e^- and τ decay data. The main qualitative lesson we have learnt is that the reduction or complete absence of such a peak and the appearance of a substantial spectral weight in the low-frequency region provide a very good description of the lattice data and are compatible with the sum rule. Moreover the area under the latter spectral weight matches the expectation of kinetic theory. This picture is corroborated by a simple phenomenological study, presented in section 2.4, based on the experimental $R(s)$ ratio

JHEP03(2013)100

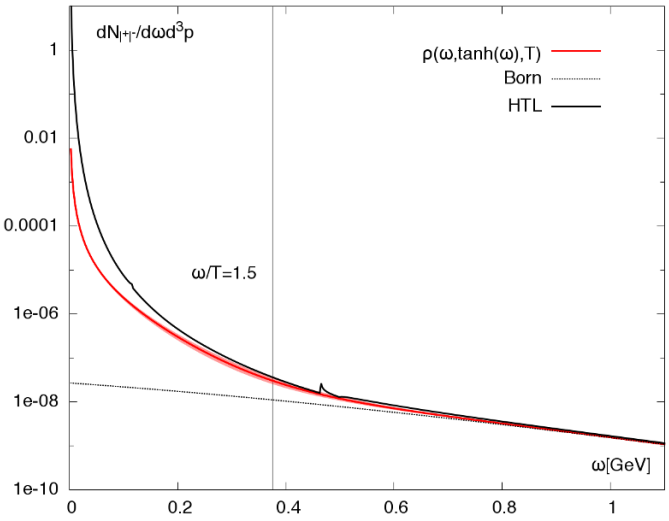

Figure 11. The production rate of lepton pairs from two-flavor lattice QCD for frequencies ω given in units [GeV] as calculated from spectral functions of the vector current using eq. (2.17). The curve comes from fitting $\rho_{ii}(\omega, T)$ to $G_{ii}(\tau, T)$ using the transport peak Ansatz 2. The black line shows the result from HTL perturbation theory with $m_T/T = 1$, while the dashed line denotes the (free) Born rate.

and the sum rule. We also note that the analytic result (2.15) in the strongly coupled limit of $\mathcal{N} = 4$ super-Yang-Mills theory exhibits a qualitatively similar (but quantitatively different in amplitude) change of sign in the difference of thermal and vacuum spectral functions, even though the theory is conformal and therefore exhibits no analogue of the ρ meson. A similar pattern was also observed in the bulk channel of the pure SU(3) gauge theory [8].

The analysis presented in this paper is based on data at finite lattice spacing. Obviously the next step would be to repeat the analysis in the continuum limit, as has been done in the quenched theory [50]. In this respect the results obtained here should be regarded as preliminary. We note however that our results are quantitatively quite close to those obtained in [50].

It would be very interesting to repeat the analysis carried out here in a temperature scan through the smooth phase transition. This would allow one to track the fate of the ρ meson from the low-temperature to the high-temperature phase and perhaps to shed light on the excess of dileptons observed by the PHENIX collaboration in relativistic gold-gold collisions [51]. The methods employed here to constrain thermal spectral functions may be useful in the context of cosmology as well, see for instance [52].

Acknowledgments

We are very grateful to Marina Marinkovic who generated the zero-temperature ensemble used here that was made available to us through CLS. We also warmly thank Georg von Hippel who provided the vector correlator on this ensemble. H.M. thanks Aleksi Vuorinen for discussions. We acknowledge the use of computing time for the generation of the gauge

JHEP03(2013)100

configurations on the JUGENE computer of the Gauss Centre for Supercomputing located at Forschungszentrum Jülich, Germany, allocated partly through the European PRACE initiative and partly through the John von Neumann Institute for Computing (NIC). In particular, the finite-temperature ensemble was generated within NIC project HMZ21. The correlation functions were computed on the dedicated QCD platform "Wilson" at the Institute for Nuclear Physics, University of Mainz. This work was supported by the *Center for Computational Sciences in Mainz* and by the DFG grant ME 3622/2-1 *Static and dynamic properties of QCD at finite temperature*.

References

[1] P.B. Arnold, G.D. Moore and L.G. Yaffe, *Photon emission from quark gluon plasma: Complete leading order results*, *JHEP* **12** (2001) 009 [hep-ph/0111107] [INSPIRE].

[2] P.B. Arnold, G.D. Moore and L.G. Yaffe, *Transport coefficients in high temperature gauge theories. 2. Beyond leading log*, *JHEP* **05** (2003) 051 [hep-ph/0302165] [INSPIRE].

[3] P.B. Arnold, C. Dogan and G.D. Moore, *The Bulk Viscosity of High-Temperature QCD*, *Phys. Rev.* **D 74** (2006) 085021 [hep-ph/0608012] [INSPIRE].

[4] D.A. Teaney, *Viscous Hydrodynamics and the Quark Gluon Plasma*, arXiv:0905.2433 [INSPIRE].

[5] H. Song, *Hydrodynamic Modeling and the QGP Shear Viscosity*, *Eur. Phys. J.* **A 48** (2012) 163 [arXiv:1207.2396] [INSPIRE].

[6] R. Rapp and J. Wambach, *Chiral symmetry restoration and dileptons in relativistic heavy ion collisions*, *Adv. Nucl. Phys.* **25** (2000) 1 [hep-ph/9909229] [INSPIRE].

[7] K. Hagiwara, R. Liao, A.D. Martin, D. Nomura and T. Teubner, $(g-2)_\mu$ *and* $\alpha(M_Z^2)$ *re-evaluated using new precise data*, *J. Phys.* **G 38** (2011) 085003 [arXiv:1105.3149] [INSPIRE].

[8] H.B. Meyer, *The Bulk Channel in Thermal Gauge Theories*, *JHEP* **04** (2010) 099 [arXiv:1002.3343] [INSPIRE].

[9] H.-T. Ding et al., *Thermal dilepton rate and electrical conductivity: An analysis of vector current correlation functions in quenched lattice QCD*, *Phys. Rev.* **D 83** (2011) 034504 [arXiv:1012.4963] [INSPIRE].

[10] H.B. Meyer, *Transport Properties of the quark-gluon Plasma: A Lattice QCD Perspective*, *Eur. Phys. J.* **A 47** (2011) 86 [arXiv:1104.3708] [INSPIRE].

[11] D. Bernecker and H.B. Meyer, *Vector Correlators in Lattice QCD: Methods and applications*, *Eur. Phys. J.* **A 47** (2011) 148 [arXiv:1107.4388] [INSPIRE].

[12] K. Chetyrkin, V. Spiridonov and S. Gorishnii, *Wilson expansion for correlators of vector currents at the two loop level: dimension four operators*, *Phys. Lett.* **B 160** (1985) 149 [INSPIRE].

[13] S. Mallik, *Operator product expansion at finite temperature*, *Phys. Lett.* **B 416** (1998) 373 [hep-ph/9710556] [INSPIRE].

[14] Y. Burnier and M. Laine, *Massive vector current correlator in thermal QCD*, *JHEP* **11** (2012) 086 [arXiv:1210.1064] [INSPIRE].

JHEP03(2013)100

[15] P. Baikov, K. Chetyrkin, J. Kuhn and J. Rittinger, *Vector Correlator in Massless QCD at Order $O(alpha_s^4)$ and the QED β-function at Five Loop*, *JHEP* **07** (2012) 017 [arXiv:1206.1284] [INSPIRE].

[16] K. Chetyrkin, R. Harlander, J.H. Kuhn and M. Steinhauser, *Mass corrections to the vector current correlator*, *Nucl. Phys.* **B 503** (1997) 339 [hep-ph/9704222] [INSPIRE].

[17] P. Petreczky and D. Teaney, *Heavy quark diffusion from the lattice*, *Phys. Rev.* **D 73** (2006) 014508 [hep-ph/0507318] [INSPIRE].

[18] G.D. Moore and J.-M. Robert, *Dileptons, spectral weights and conductivity in the quark-gluon plasma*, hep-ph/0607172 [INSPIRE].

[19] J. Hong and D. Teaney, *Spectral densities for hot QCD plasmas in a leading log approximation*, *Phys. Rev.* **C 82** (2010) 044908 [arXiv:1003.0699] [INSPIRE].

[20] R.C. Myers, A.O. Starinets and R.M. Thomson, *Holographic spectral functions and diffusion constants for fundamental matter*, *JHEP* **11** (2007) 091 [arXiv:0706.0162] [INSPIRE].

[21] L.D. McLerran and T. Toimela, *Photon and Dilepton Emission from the quark-gluon Plasma: Some General Considerations*, *Phys. Rev.* **D 31** (1985) 545 [INSPIRE].

[22] F. Jegerlehner and R. Szafron, *$\rho^0 - \gamma$ mixing in the neutral channel pion form factor F_π^e and its role in comparing e^+e^- with τ spectral functions*, *Eur. Phys. J.* **C 71** (2011) 1632 [arXiv:1101.2872] [INSPIRE].

[23] S. Borsányi et al., *Fluctuations of conserved charges at finite temperature from lattice QCD*, *JHEP* **01** (2012) 138 [arXiv:1112.4416] [INSPIRE].

[24] S. Caron-Huot, *Asymptotics of thermal spectral functions*, *Phys. Rev.* **D 79** (2009) 125009 [arXiv:0903.3958] [INSPIRE].

[25] M. Hasenbusch, *Speeding up the hybrid Monte Carlo algorithm for dynamical fermions*, *Phys. Lett.* **B 519** (2001) 177 [hep-lat/0107019] [INSPIRE].

[26] M. Hasenbusch and K. Jansen, *Speeding up lattice QCD simulations with clover improved Wilson fermions*, *Nucl. Phys.* **B 659** (2003) 299 [hep-lat/0211042] [INSPIRE].

[27] M. Marinkovic and S. Schaefer, *Comparison of the mass preconditioned HMC and the DD-HMC algorithm for two-flavour QCD*, PoS(LATTICE2010)031 [arXiv:1011.0911] [INSPIRE].

[28] http://luscher.web.cern.ch/luscher/DD-HMC/index.html, (2010)

[29] https://twiki.cern.ch/twiki/bin/view/CLS/WebIntro, (2010).

[30] K.G. Wilson, *Confinement of Quarks*, *Phys. Rev.* **D 10** (1974) 2445 [INSPIRE].

[31] ALPHA collaboration, K. Jansen and R. Sommer, *O(alpha) improvement of lattice QCD with two flavors of Wilson quarks*, *Nucl. Phys.* **B 530** (1998) 185 [*Erratum ibid.* **B 643** (2002) 517-518] [hep-lat/9803017] [INSPIRE].

[32] P. Fritzsch et al., *The strange quark mass and Lambda parameter of two flavor QCD*, *Nucl. Phys.* **B 865** (2012) 397 [arXiv:1205.5380] [INSPIRE].

[33] B.B. Brandt, A. Francis, H.B. Meyer, H. Wittig and O. Philipsen, *QCD thermodynamics with two flavours of Wilson fermions on large lattices*, PoS(LATTICE2012)073 [arXiv:1210.6972] [INSPIRE].

[34] M. Lüscher, S. Sint, R. Sommer and P. Weisz, *Chiral symmetry and O(a) improvement in lattice QCD*, *Nucl. Phys.* **B 478** (1996) 365 [hep-lat/9605038] [INSPIRE].

JHEP03(2013)100

[35] S. Sint and P. Weisz, *Further results on O(a) improved lattice QCD to one loop order of perturbation theory*, *Nucl. Phys.* **B 502** (1997) 251 [hep-lat/9704001] [INSPIRE].

[36] M. Della Morte, R. Hoffmann, F. Knechtli, R. Sommer and U. Wolff, *Non-perturbative renormalization of the axial current with dynamical Wilson fermions*, *JHEP* **07** (2005) 007 [hep-lat/0505026] [INSPIRE].

[37] M. Lüscher, *Signatures of unstable particles in finite volume*, *Nucl. Phys.* **B 364** (1991) 237 [INSPIRE].

[38] H.B. Meyer, *Lattice QCD and the Timelike Pion Form Factor*, *Phys. Rev. Lett.* **107** (2011) 072002 [arXiv:1105.1892] [INSPIRE].

[39] G. Aarts and J.M. Martinez Resco, *Continuum and lattice meson spectral functions at nonzero momentum and high temperature*, *Nucl. Phys.* **B 726** (2005) 93 [hep-lat/0507004] [INSPIRE].

[40] W. Florkowski and B.L. Friman, *Spatial dependence of the finite temperature meson correlation function*, *Z. Phys.* **A 347** (1994) 271 [INSPIRE].

[41] G. Aarts and J.M. Martinez Resco, *Transport coefficients, spectral functions and the lattice*, *JHEP* **04** (2002) 053 [hep-ph/0203177] [INSPIRE].

[42] G. Aarts and J.M. Martinez Resco, *Transport coefficients from the lattice?*, *Nucl. Phys. Proc. Suppl.* **119** (2003) 505 [hep-lat/0209033] [INSPIRE].

[43] Y. Burnier and M. Laine, *Towards flavour diffusion coefficient and electrical conductivity without ultraviolet contamination*, *Eur. Phys. J.* **C 72** (2012) 1902 [arXiv:1201.1994] [INSPIRE].

[44] S. Gupta, *The Electrical conductivity and soft photon emissivity of the QCD plasma*, *Phys. Lett.* **B 597** (2004) 57 [hep-lat/0301006] [INSPIRE].

[45] G. Aarts, C. Allton, J. Foley, S. Hands and S. Kim, *Spectral functions at small energies and the electrical conductivity in hot, quenched lattice QCD*, *Phys. Rev. Lett.* **99** (2007) 022002 [hep-lat/0703008] [INSPIRE].

[46] E. Braaten and R.D. Pisarski, *Soft Amplitudes in Hot Gauge Theories: A General Analysis*, *Nucl. Phys.* **B 337** (1990) 569 [INSPIRE].

[47] R. Rapp, *In-Medium Vector Mesons, Dileptons and Chiral Restoration*, *AIP Conf. Proc.* **1322** (2010) 55 [arXiv:1010.1719] [INSPIRE].

[48] R. Baier, S.A. Stricker, O. Taanila and A. Vuorinen, *Production of Prompt Photons: Holographic Duality and Thermalization*, *Phys. Rev.* **D 86** (2012) 081901 [arXiv:1207.1116] [INSPIRE].

[49] R. Baier, S.A. Stricker, O. Taanila and A. Vuorinen, *Holographic Dilepton Production in a Thermalizing Plasma*, *JHEP* **07** (2012) 094 [arXiv:1205.2998] [INSPIRE].

[50] A. Francis, *Thermal Dilepton Rates from Quenched Lattice QCD*, PhD. Thesis, Universität Bielefeld (2011), http://pub.uni-bielefeld.de/download/2403291/2403313.

[51] PHENIX collaboration, A. Adare et al., *Detailed measurement of the e^+e^- pair continuum in $p+p$ and Au+Au collisions at $\sqrt{s_{NN}} = 200$ GeV and implications for direct photon production*, *Phys. Rev.* **C 81** (2010) 034911 [arXiv:0912.0244] [INSPIRE].

[52] T. Asaka, M. Laine and M. Shaposhnikov, *On the hadronic contribution to sterile neutrino production*, *JHEP* **06** (2006) 053 [hep-ph/0605209] [INSPIRE].

JHEP03(2013)100